

# System-size dependence of the viscous attenuation of anisotropic flow in p+Pb and Pb+Pb collisions at LHC energies

Peifeng Liu<sup>1,2</sup> and Roy A. Lacey<sup>1,2,\*</sup>

<sup>1</sup>*Department of Chemistry, Stony Brook University,  
Stony Brook, NY, 11794-3400, USA*

<sup>2</sup>*Department of Physics and Astronomy, Stony Brook University,  
Stony Brook, NY, 11794-3800*

(Dated: January 3, 2019)

The elliptic and triangular flow coefficients ( $v_n$ ,  $n = 2, 3$ ) measured in Pb+Pb ( $\sqrt{s_{NN}} = 2.76$  TeV) and p+Pb ( $\sqrt{s_{NN}} = 5.02$  TeV) collisions, are studied as a function of initial-state eccentricity ( $\varepsilon_n$ ), and dimensionless size characterized by the cube root of the mid-rapidity charged hadron multiplicity density  $\langle N_{ch} \rangle^{1/3}$ . The results indicate that the influence of eccentricity ( $v_n \propto \varepsilon_n$ ) observed for large  $\langle N_{ch} \rangle$ , is superseded by the effects of viscous attenuation at small  $\langle N_{ch} \rangle$ . However, strikingly similar acoustic scaling patterns of exponential viscous modulation, with a damping rate proportional to  $n^2$  and inversely proportional to the dimensionless size, are observed for the p+Pb and Pb+Pb eccentricity-scaled coefficients. The resulting scaling parameters suggest that, contrary to current predilections, the patterns of viscous attenuation and the specific shear viscosities  $\langle \eta/s(T) \rangle$ , for the high energy density matter created in these p+Pb and Pb+Pb collisions, are comparable.

PACS numbers:

Relativistic heavy-ion collisions can lead to the production of high energy density domains of strongly interacting matter with an anisotropic transverse energy density profile. The ensuing expansion and hadronization of this so-called fireball of dense partonic matter, results in the production of particles with an azimuthal anisotropy that reflects the viscous hydrodynamic response to the initial anisotropic energy density profile [1–10].

The shape of this energy density profile  $\rho_e(r, \varphi)$ , can be characterized by the complex eccentricity vectors [11–15]:

$$\mathcal{E}_n \equiv \varepsilon_n e^{in\Phi_n} \equiv -\frac{\int d^2r_\perp r^m e^{in\varphi} \rho_e(r, \varphi)}{\int d^2r_\perp r^m \rho_e(r, \varphi)}, \quad (1)$$

where  $\varepsilon_n = \langle |\mathcal{E}_n|^2 \rangle^{1/2}$  and  $\Phi_n$  denote the magnitude and azimuthal direction of the  $n^{\text{th}}$ -order eccentricity vector which fluctuates from event to event;  $m = n$  for  $n \geq 2$  and  $m = 3$  for  $n = 1$  [14, 16, 17].

The anisotropic flow which derives from  $\varepsilon_n$ , results in an azimuthal asymmetry of the measured single-particle distribution. Thus, it can be quantified by the complex flow vectors [18–20]:

$$V_n \equiv v_n e^{in\Psi_n} \equiv \langle e^{in\phi} \rangle, \quad v_n = \langle |V_n|^2 \rangle^{1/2}, \quad (2)$$

where  $\phi$  denotes the azimuthal angle around the beam direction, of a particle emitted in the collision,  $\{ \dots \}$  denotes the average over all particles emitted in the event, and  $v_n$  and  $\Psi_n$  denote the magnitude and azimuthal direction of the  $n^{\text{th}}$ -order harmonic flow vector which also fluctuates from event to event.

Viscous hydrodynamical model investigations show that  $v_n \propto \varepsilon_n$  for elliptic and triangular flow ( $n = 2$  and  $3$ ) for the “large” and moderate-sized systems produced in

heavy ion collisions [10, 15, 21–23]. They also indicate that the temperature dependent specific shear viscosity (i.e., the ratio of shear viscosity to entropy density  $\eta/s(T)$ ) of the partonic medium produced in the collisions, serve to attenuate the magnitude of  $v_n$  and consequently the ratio  $v_n/\varepsilon_n$ . Thus, viscous hydrodynamical model comparisons to  $v_n$  measurements have been, and continue to be an important avenue to estimate the value of  $\eta/s(T)$  [2, 3, 5, 7, 9, 10, 15, 24–27] for the partonic matter produced in the large to moderate-sized systems created in central and mid-central heavy ion collisions.

For the small systems produced in peripheral heavy ion collisions and light-heavy ion collisions (eg. proton–nucleus collisions), there has been a pervasive predilection for the notion that collective flow does not develop because viscous hydrodynamically-driven expansion breaks down. In part, this notion stems from the expectation that microscopic scales such as the mean free path, are probably similar to the geometric size of these systems. Thus, the presence of the large gradients inherent to small systems, could excite non-hydrodynamic modes or render invalid, the hydrodynamic gradient expansion required to accurately characterize the viscous hydrodynamic response. It has also been argued that alternative mechanistic scenarios, such as initial state correlations [28–30], could account for the azimuthal anisotropy observed for these small systems. A decisive validation of such scenarios would make the question of the validity of viscous hydrodynamical evolution in small systems a moot point.

Recent experimental measurements at both RHIC [31, 32] and the LHC [33–35], have given strong indications for collective anisotropic flow in the small systems produced in peripheral heavy ion collisions and light-heavy

ion collisions. Several attempts have also been made to reconcile these measurements with viscous hydrodynamical evolution of the high energy-density strongly interacting matter which comprise these systems [36–39]. However, the disparate influence of initial-state eccentricity, system size and  $\eta/s(T)$  has not been fully charted for these systems. Currently, it is also unclear as to what constitutes a good experimental measure of the size of these systems, as well as how small they can be and still hydrodynamize. For the latter, numerical simulations in strongly interacting theories suggests that hydrodynamics remains applicable when the system size ( $R$ ) is of  $\mathcal{O}(1/T)$  – the inverse temperature. That is, when the dimensionless size  $RT \sim 1$  [40].

The respective influence of  $\varepsilon_n$ , system size and  $\eta/s(T)$  on  $v_n$ , can be studied within an acoustic model framework, akin to that of relativistic viscous hydrodynamics [8, 41–44]. Within this framework, the viscous attenuation of  $v_n$  for a given mean transverse momentum  $\langle p_T \rangle$  and centrality selection cent, can be expressed as [8, 41–44]:

$$\frac{v_n}{\varepsilon_n} \propto \exp\left(-n^2 \beta \frac{1}{RT}\right) \quad n = 2, 3, \quad (3)$$

where  $\beta \propto \eta/s(T)$  and  $R$  characterizes the geometric size of the medium produced in the collision. For a given centrality selection, the dimensionless size  $RT \propto \langle N_{ch} \rangle^{1/3}$ , where  $\langle N_{ch} \rangle$  is the mid-rapidity charged hadron multiplicity density [45].

Equation 3 suggests characteristic linear dependencies for  $\ln(v_n/\varepsilon_n)$  and  $\ln[(v_3/\varepsilon_3)/(v_2/\varepsilon_2)]$  on  $\langle N_{ch} \rangle^{-1/3}$ , with slopes that reflect the quadratic viscous attenuation prefactors for  $\beta$ ; these combined features are termed acoustic scaling. Since  $\langle N_{ch} \rangle$  is small for peripheral heavy ion collisions and light-heavy ion collisions, Eq. 3 also suggests that an uncharacteristically large viscous suppression of  $v_n$  (relative to that for large systems) is to be expected for the small systems of dimensionless size  $RT \propto \langle N_{ch} \rangle^{1/3}$ , produced in these collisions.

An observed similarity in the slopes for  $\ln[(v_3/\varepsilon_3)/(v_2/\varepsilon_2)]$  vs.  $\langle N_{ch} \rangle^{-1/3}$ , for both small and large systems, would not only confirm that  $\langle N_{ch} \rangle^{1/3}$  is a good measure for the dimensionless size, but would also indicate that  $\eta/s(T)$  for the medium produced in these systems are comparable. Thus, the validation of acoustic scaling for  $v_n/\varepsilon_n$  across the full range of dimensionless sizes afforded in Pb+Pb and p+Pb collisions, could provide further constraints for the range of applicability of viscous hydrodynamics, as well as aid its utility for precision extraction of  $\eta/s(T)$ .

In this letter, we use recent  $p_T$ -integrated ( $0.3 < p_T < 3$  GeV/c)  $v_2$  and  $v_3$  measurements in Pb+Pb ( $\sqrt{s_{NN}} = 2.76$  TeV) and p+Pb ( $\sqrt{s_{NN}} = 5.02$  TeV) collisions, to explore validation tests for acoustic scaling of  $v_n/\varepsilon_n$  and the ratio  $(v_3/\varepsilon_3)/(v_2/\varepsilon_2)$ . We find

that these tests provide crucial insight on the influence of system size on viscous hydrodynamic evolution. Additionally, they allow a direct comparison of  $\langle \eta/s(T) \rangle$  for the hot and dense medium produced in p+Pb and Pb+Pb collisions, over the full range of system sizes characterized by the dimensionless size  $RT \propto \langle N_{ch} \rangle^{1/3}$ .

The data employed in this work are taken from the CMS centrality selected flow measurements for Pb+Pb collisions at  $\sqrt{s_{NN}} = 2.76$  TeV [46, 47] and the CMS  $N_{ch}$ -selected flow measurements for Pb+Pb collisions at  $\sqrt{s_{NN}} = 2.76$  TeV and p+Pb collisions at  $\sqrt{s_{NN}} = 5.02$  TeV [33]. The  $N_{ch}$  selections for the latter measurements were made for 2.4 units of pseudorapidity (i.e.,  $|\eta| < 2.4$ ). Consequently, the efficiency corrected values were scaled to obtain  $\langle N_{ch} \rangle$  for one unit of  $\eta$ , to ensure consistency with the centrality dependent measurements. The requisite  $\langle N_{ch} \rangle$  values for the centrality selected measurements were obtained from the CMS multiplicity density measurements [48].

The requisite  $\langle N_{ch} \rangle$  dependent eccentricities were calculated following the procedure outlined in Eq. 1, with the aid of a Monte Carlo quark-Glauber model (MC-qGlauber) with fluctuating initial conditions [49]. The model, which is based on the commonly used MC-Glauber model [50], was used to compute the number of quark participants  $N_{qpart}(cent)$ ,  $\varepsilon_n(cent)$  and  $\varepsilon_n(\langle N_{ch} \rangle)$  from the two-dimensional profile of the density of sources in the transverse plane  $\rho_s(\mathbf{r}_\perp)$  [13, 20, 49]. The model takes account of the finite size of the nucleon, the wounding profile of the nucleon, the distribution of quarks inside the nucleon and quark cross sections which reproduce the NN inelastic cross section at  $\sqrt{s_{NN}} = 2.76$  and 5.02 TeV. A systematic uncertainty of 2-5% was estimated for the eccentricities from variations of the model parameters.

Validation tests for acoustic scaling were performed by plotting  $v_n/\varepsilon_n$  and  $(v_3/\varepsilon_3)/(v_2/\varepsilon_2)$  vs.  $\langle N_{ch} \rangle^{-1/3}$  respectively, followed by evaluations for the expected patterns of exponential viscous attenuation, and the relative viscous attenuation  $\beta$ -prefactors indicated in Eq. 3.

Figure 1(a) shows the  $\langle N_{ch} \rangle$  dependence of  $v_2$  and  $v_3$  for the combined data sets for Pb+Pb collisions, as well as the  $\langle N_{ch} \rangle$  dependence of  $\varepsilon_2$  and  $\varepsilon_3$ . To facilitate a comparison between  $v_n$  and  $\varepsilon_n$ , the  $\varepsilon_n$  values are divided by a factor to normalize  $v_n$  and  $\varepsilon_n$  at  $\langle N_{ch} \rangle \sim 1600$ . Fig. 1(a) shows that, for  $\langle N_{ch} \rangle \gtrsim 400$ ,  $v_n$  follows the trend for  $\varepsilon_n$ , i.e.,  $v_n \propto \varepsilon_n$ . However, for  $\langle N_{ch} \rangle \lesssim 400$ , the  $v_n$  trend is opposite to that for  $\varepsilon_n$ . We attribute this striking difference in trend, to the very large viscous attenuation effects which result for small system sizes. That is, for small dimensionless sizes, the expectation that  $v_n \propto \varepsilon_n$  is superseded by the dominating effects of the exponential viscous attenuation implied in Eq. 3.

This pattern of exponential viscous attenuation is made transparent in Figs. 1(b) and (c), which show the telltale acoustic scaling patterns of a characteristic lin-

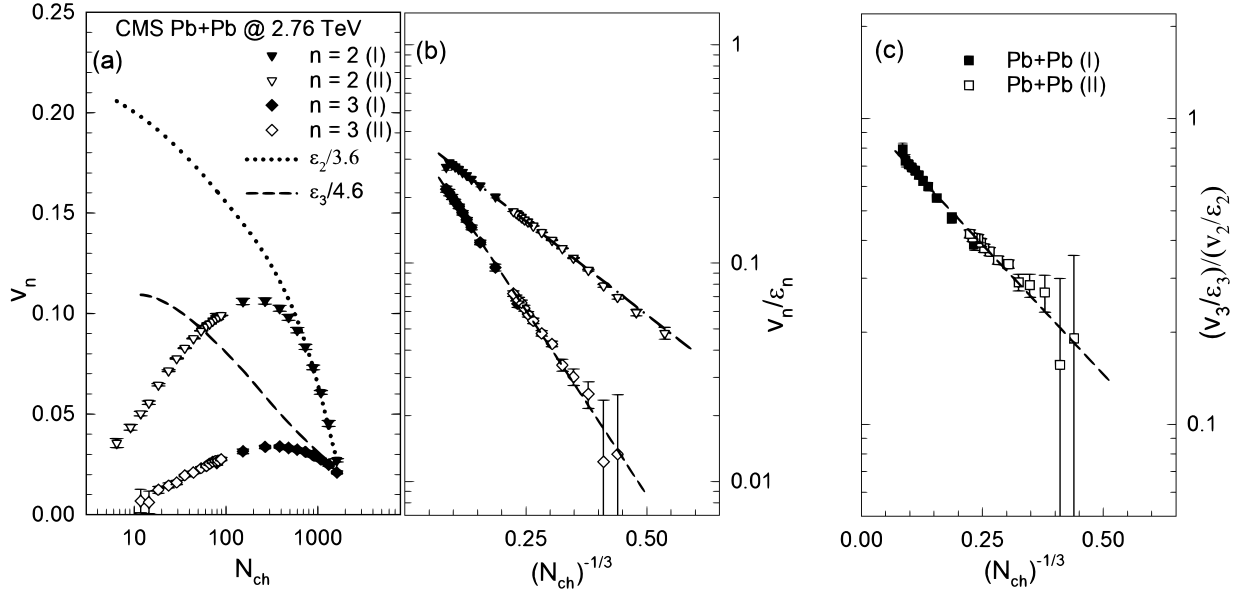


FIG. 1. (a)  $v_n$  and  $\epsilon_n$  vs.  $\langle N_{ch} \rangle$  for Pb+Pb collisions at  $\sqrt{s_{NN}} = 2.76$ . The filled and open symbols indicate centrality selected (I) and  $N_{ch}$ -selected (II) measurements respectively. The dotted and dashed curves show  $\epsilon_n$  values which are normalized to  $v_n$  at  $\langle N_{ch} \rangle \sim 1600$ ; (b)  $v_n/\epsilon_n$  vs.  $(\langle N_{ch} \rangle)^{-1/3}$  for the data shown in panel (a). The dashed lines represent fits to the eccentricity-scaled data following Eq. 3; (c)  $[(v_3/\epsilon_3)/(v_2/\epsilon_2)]$  vs.  $(\langle N_{ch} \rangle)^{-1/3}$  for the data shown in panel (b). The dashed line represents a fit to the data following Eq. 3.

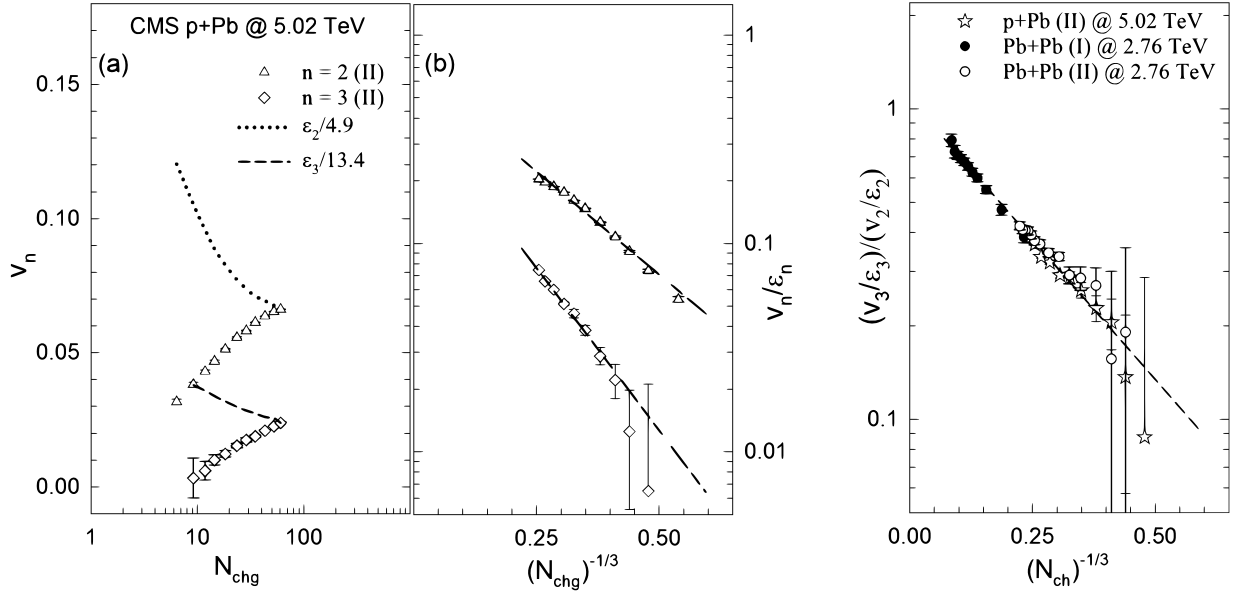


FIG. 2. (a)  $v_n$  and  $\epsilon_n$  vs.  $\langle N_{ch} \rangle$  for  $N_{ch}$ -selected (II) measurements of  $v_n$  in p+Pb collisions at  $\sqrt{s_{NN}} = 5.02$  TeV. The dotted and dashed curves show  $\epsilon_n$  values which are normalized to  $v_n$  at  $\langle N_{ch} \rangle \sim 60$ ; (b)  $v_n/\epsilon_n$  vs.  $(\langle N_{ch} \rangle)^{-1/3}$  for the data shown in panel (a). The dashed lines represent fits to the eccentricity-scaled data following Eq. 3; (c)  $\ln[(v_3/\epsilon_3)/(v_2/\epsilon_2)]$  vs.  $(\langle N_{ch} \rangle)^{-1/3}$  for the data shown in panel (b). The dashed line represents a fit to the data following Eq. 3.

ear dependence of  $\ln(v_n/\epsilon_n)$  and  $\ln[(v_3/\epsilon_3)/(v_2/\epsilon_2)]$  on  $(\langle N_{ch} \rangle)^{-1/3}$  (respectively), with slope factors which reflect the  $n^2$  dependence on harmonic number. Note that the  $\beta$ -prefactors (indicated in Eq. 3) for  $\ln(v_n/\epsilon_n)$  vs.  $(\langle N_{ch} \rangle)^{-1/3}$  are 4 and 9 for  $n = 2$  and 3 respectively, and the prefactor

for  $\ln[(v_3/\epsilon_3)/(v_2/\epsilon_2)]$  vs.  $(\langle N_{ch} \rangle)^{-1/3}$  is 5. Note as well that the ratio  $(v_3/\epsilon_3)/(v_2/\epsilon_2)$  leads to a significant reduction in the influence of possible  $p_T$ -dependent viscous effects [44] for the  $\langle p_T \rangle$  values of interest.

The dashed lines in Figs. 1(b) and (c) represent fits

to the eccentricity-scaled data following Eq. 3. They indicate relatively good fits which suggest a common  $\langle\eta/s(T)\rangle$  for the full range of system sizes spanned by the combined data sets for these Pb+Pb collisions. This could be an indication for a weak temperature dependence of  $\eta/s$  at LHC energies [10]. It is noteworthy that this size-independent value of the  $\langle\eta/s(T)\rangle$ , results in viscous attenuation which is significantly larger in small systems than in large systems (cf. Figs. 1(b) and (c)).

The results obtained for the  $N_{\text{ch}}$ -selected measurements for p+Pb are shown in Fig. 2. They indicate strikingly similar patterns to the ones shown in Fig. 1 for the  $N_{\text{ch}}$ -selected Pb+Pb data, albeit with different magnitudes for  $v_n$  and  $\varepsilon_n$ . Fig. 2(a) shows that the  $\langle N_{\text{ch}} \rangle$  dependence of  $v_n$  is opposite to the trend for  $\varepsilon_n$  over the full range of the measurements. Here, the  $\varepsilon_n$  values are also divided by the indicated factors to normalize  $v_n$  and  $\varepsilon_n$  at  $\langle N_{\text{ch}} \rangle \sim 60$ . The statistical significance of the  $\varepsilon_n$  values, precluded a comparison for larger  $\langle N_{\text{ch}} \rangle$  values. Note that the  $\langle N_{\text{ch}} \rangle$  values in Fig. 2 are for one unit of pseudorapidity. The observed trends confirm that the very large viscous attenuation effects, apparent for the small systems created in Pb+Pb collisions (c.f. Fig. 1), are also present in p+Pb collisions for comparable  $\langle N_{\text{ch}} \rangle$ .

The revealing acoustic scaling patterns of a characteristic linear dependence of  $\ln(v_n/\varepsilon_n)$  and  $\ln[(v_3/\varepsilon_3)/(v_2/\varepsilon_2)]$  on  $(N_{\text{ch}})^{-1/3}$  (respectively), with slope factors which reflect the  $n^2$  dependence on harmonic number, are also apparent in Figs. 2(b) and (c). They are strikingly similar to the scaling patterns previously observed in Figs. 1(b) and (c) for Pb+Pb collisions. The indicated dashed lines, which represent fits to the eccentricity-scaled data (following Eq. 3), also suggest a common  $\langle\eta/s(T)\rangle$  over the full range of system sizes obtained with different selections of  $\langle N_{\text{ch}} \rangle$ . Here, it should be emphasized again that this implied size-independence of the  $\langle\eta/s(T)\rangle$  for the medium produced in p+Pb systems of varying sizes, are compatible with the large size-dependent viscous attenuation effects produced in these collisions.

The size dependence of the ratio of the eccentricity-scaled coefficients  $(v_3/\varepsilon_3)/(v_2/\varepsilon_2)$ , for the p+Pb and Pb+Pb measurements are compared in Fig. 3. Note that this ratio leads to a significant reduction in the influence of possible  $p_T$  dependent viscous effects [44] which could be different for p+Pb and Pb+Pb collisions. The comparison indicates strikingly similar magnitudes and trends for both sets of measurements. The dashed line, which represent the results from a fit to the combined data sets, indicate that, within an uncertainty of  $\sim 6\%$ , a single slope value  $\beta = 0.83 \pm 0.05$ , can account for the wealth of the combined measurements. To estimate the fit uncertainty, independent fits were performed for each data set.

The observed similarity between the extracted slopes for p+Pb and Pb+Pb results, suggests that the  $\langle\eta/s(T)\rangle$

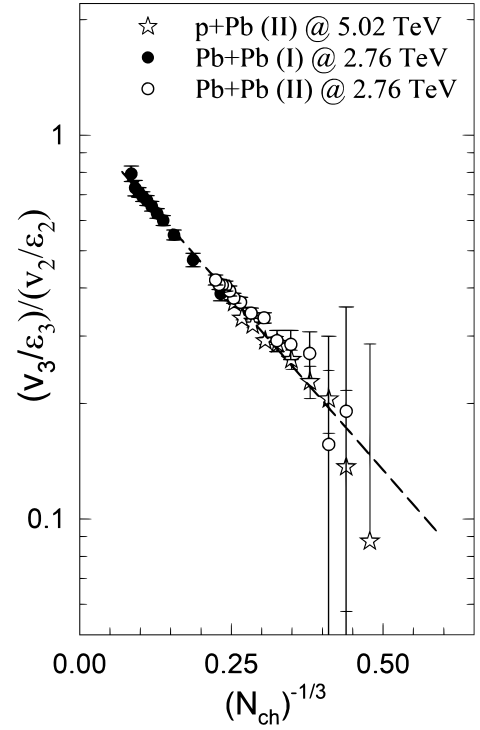


FIG. 3. Comparison of  $\ln[(v_3/\varepsilon_3)/(v_2/\varepsilon_2)]$  vs.  $\langle N_{\text{ch}} \rangle^{-1/3}$  for centrality selected (I) and  $N_{\text{ch}}$ -selected (II) Pb+Pb measurements, and  $N_{\text{ch}}$ -selected (II) p+Pb measurements. The dashed line represents a fit to the combined data sets, following Eq. 3.

for the medium created in p+Pb and Pb+Pb collisions are comparable. However, a further calibration that maps the extracted value of  $\beta$  on to the value for the  $\langle\eta/s(T)\rangle$  would be required. An appropriately constrained set of viscous hydrodynamical calculations, tuned to reproduce the results shown in Figs. 1 - 3, could provide such a calibration to give a relatively precise estimate, as well as simultaneous validation of the initial-state eccentricity spectrum for these collisions.

In summary, we have presented a detailed phenomenological investigation of the influence of dimensionless size ( $RT \propto \langle N_{\text{ch}} \rangle^{1/3}$ ) on the viscous attenuation of the elliptic and triangular flow coefficients measured in Pb+Pb ( $\sqrt{s_{\text{NN}}} = 2.76$  TeV) and p+Pb ( $\sqrt{s_{\text{NN}}} = 5.02$  TeV) collisions. We find that, for small  $\langle N_{\text{ch}} \rangle$  (small dimensionless size), the magnitude of the flow coefficients are dominated by the effects of size-driven viscous attenuation. Strikingly similar acoustic scaling patterns of exponential viscous modulation, with a damping rate proportional to  $n^2$  and inversely proportional to the dimensionless size, are observed for both the p+Pb and Pb+Pb eccentricity-scaled coefficients. Such patterns suggest that the very large viscous attenuation effects, apparent in the small systems created in p+Pb collisions are also present in Pb+Pb collisions of comparable  $\langle N_{\text{ch}} \rangle$ . The scaling parameters for the ratio of the eccentricity-scaled  $v_n$  coefficients



cients, further suggests comparable size-independent specific shear viscosities  $\langle\eta/s(T)\rangle$  for the hot and dense matter produced in p+Pb and Pb+Pb collisions, contrary to current predilections. These results could provide additional stringent constraints for the range of applicability of viscous hydrodynamics, as well as to aid its utility for precision extraction of the transport coefficients for hot and dense partonic matter.

**Acknowledgments** This research is supported by the US DOE under contract DE-FG02-87ER40331.A008.

---

\* E-mail: Roy.Lacey@Stonybrook.edu

- [1] D. Teaney, *Phys.Rev.* **C68**, 034913 (2003), [arXiv:nucl-th/0301099 \[nucl-th\]](#).
- [2] P. Romatschke and U. Romatschke, *Phys.Rev.Lett.* **99**, 172301 (2007), [arXiv:0706.1522 \[nucl-th\]](#).
- [3] H. Song, S. A. Bass, U. Heinz, T. Hirano, and C. Shen, *Phys. Rev. Lett.* **106**, 192301 (2011), [Erratum: *Phys. Rev. Lett.* 109, 139904 (2012)], [arXiv:1011.2783 \[nucl-th\]](#).
- [4] J. Qian, U. W. Heinz, and J. Liu, *Phys. Rev.* **C93**, 064901 (2016), [arXiv:1602.02813 \[nucl-th\]](#).
- [5] B. Schenke, S. Jeon, and C. Gale, *Phys.Lett.* **B702**, 59 (2011), [arXiv:1102.0575 \[hep-ph\]](#).
- [6] P. Bozek, *Phys. Rev.* **C85**, 014911 (2012), [arXiv:1112.0915 \[hep-ph\]](#).
- [7] F. G. Gardim, F. Grassi, M. Luzum, and J.-Y. Ollitrault, *Phys.Rev.Lett.* **109**, 202302 (2012), [arXiv:1203.2882 \[nucl-th\]](#).
- [8] E. Shuryak and I. Zahed, (2013), [arXiv:1301.4470 \[hep-ph\]](#).
- [9] S. McDonald, C. Shen, F. Fillion-Gourdeau, S. Jeon, and C. Gale, *Phys. Rev.* **C95**, 064913 (2017), [arXiv:1609.02958 \[hep-ph\]](#).
- [10] J. E. Bernhard, J. S. Moreland, S. A. Bass, J. Liu, and U. Heinz, (2016), [arXiv:1605.03954 \[nucl-th\]](#).
- [11] B. H. Alver, C. Gombeaud, M. Luzum, and J.-Y. Ollitrault, *Phys. Rev.* **C82**, 034913 (2010), [arXiv:1007.5469 \[nucl-th\]](#).
- [12] H. Petersen, G.-Y. Qin, S. A. Bass, and B. Muller, *Phys. Rev.* **C82**, 041901 (2010), [arXiv:1008.0625 \[nucl-th\]](#).
- [13] R. A. Lacey, R. Wei, N. N. Ajitanand, and A. Taranenko, *Phys. Rev.* **C83**, 044902 (2011), [arXiv:1009.5230 \[nucl-ex\]](#).
- [14] D. Teaney and L. Yan, *Phys. Rev.* **C83**, 064904 (2011), [arXiv:1010.1876 \[nucl-th\]](#).
- [15] Z. Qiu and U. W. Heinz, *Phys. Rev.* **C84**, 024911 (2011), [arXiv:1104.0650 \[nucl-th\]](#).
- [16] R. S. Bhalerao, J.-Y. Ollitrault, and S. Pal, *Phys. Lett.* **B742**, 94 (2015), [arXiv:1411.5160 \[nucl-th\]](#).
- [17] L. Yan and J.-Y. Ollitrault, *Phys. Lett.* **B744**, 82 (2015), [arXiv:1502.02502 \[nucl-th\]](#).
- [18] J.-Y. Ollitrault, *Phys. Rev.* **D46**, 229 (1992).
- [19] M. Luzum, *J. Phys.* **G38**, 124026 (2011), [arXiv:1107.0592 \[nucl-th\]](#).
- [20] D. Teaney and L. Yan, *Phys. Rev.* **C86**, 044908 (2012), [arXiv:1206.1905 \[nucl-th\]](#).
- [21] J. Fu, *Phys. Rev.* **C92**, 024904 (2015).
- [22] H. Niemi, K. J. Eskola, and R. Paatelainen, *Phys. Rev.* **C93**, 024907 (2016), [arXiv:1505.02677 \[hep-ph\]](#).
- [23] J. Noronha-Hostler, L. Yan, F. G. Gardim, and J.-Y. Ollitrault, *Phys. Rev.* **C93**, 014909 (2016), [arXiv:1511.03896 \[nucl-th\]](#).
- [24] T. Hirano, U. W. Heinz, D. Kharzeev, R. Lacey, and Y. Nara, *Phys.Lett.* **B636**, 299 (2006), [arXiv:nucl-th/0511046 \[nucl-th\]](#).
- [25] B. Schenke, S. Jeon, and C. Gale, *Phys.Rev.Lett.* **106**, 042301 (2011), [arXiv:1009.3244 \[hep-ph\]](#).
- [26] P. Bozek, M. Chojnacki, W. Florkowski, and B. Tomasik, *Phys.Lett.* **B694**, 238 (2010), [arXiv:1007.2294 \[nucl-th\]](#).
- [27] H. Niemi, G. Denicol, P. Huovinen, E. Molnar, and D. Rischke, *Phys.Rev.* **C86**, 014909 (2012), [arXiv:1203.2452 \[nucl-th\]](#).
- [28] K. Dusling and R. Venugopalan, *Phys. Rev. Lett.* **108**, 262001 (2012), [arXiv:1201.2658 \[hep-ph\]](#).
- [29] Y. V. Kovchegov and D. E. Wertepny, *Proceedings, QCD Evolution Workshop: Newport News, VA, May 6-10, 2014*, *Int. J. Mod. Phys. Conf. Ser.* **25**, 1460023 (2014).
- [30] A. Kovner and M. Lublinsky, *Int. J. Mod. Phys.* **E22**, 1330001 (2013), [arXiv:1211.1928 \[hep-ph\]](#).
- [31] A. Adare et al. (PHENIX), *Phys. Rev. Lett.* **111**, 212301 (2013), [arXiv:1303.1794 \[nucl-ex\]](#).
- [32] A. Adare et al. (PHENIX), *Phys. Rev. Lett.* **115**, 142301 (2015), [arXiv:1507.06273 \[nucl-ex\]](#).
- [33] S. Chatrchyan et al. (CMS), *Phys. Lett.* **B724**, 213 (2013), [arXiv:1305.0609 \[nucl-ex\]](#).
- [34] B. Abelev et al. (ALICE), *Phys. Lett.* **B719**, 29 (2013), [arXiv:1212.2001 \[nucl-ex\]](#).
- [35] G. Aad et al. (ATLAS), *Phys. Rev. Lett.* **110**, 182302 (2013), [arXiv:1212.5198 \[hep-ex\]](#).
- [36] P. Bozek and W. Broniowski, *Phys. Lett.* **B718**, 1557 (2013), [arXiv:1211.0845 \[nucl-th\]](#).
- [37] A. Bzdak, B. Schenke, P. Tribedy, and R. Venugopalan, *Phys. Rev.* **C87**, 064906 (2013), [arXiv:1304.3403 \[nucl-th\]](#).
- [38] B. Schenke and R. Venugopalan, *Phys. Rev. Lett.* **113**, 102301 (2014), [arXiv:1405.3605 \[nucl-th\]](#).
- [39] M. Habich, G. A. Miller, P. Romatschke, and W. Xiang, *Eur. Phys. J.* **C76**, 408 (2016), [arXiv:1512.05354 \[nucl-th\]](#).
- [40] P. Chesler, *JHEP* **03**, 146 (2016), [arXiv:1601.01583 \[hep-th\]](#).
- [41] R. A. Lacey, A. Taranenko, N. Ajitanand, and J. Alexander, (2011), [arXiv:1105.3782 \[nucl-ex\]](#).
- [42] R. A. Lacey, Y. Gu, X. Gong, D. Reynolds, N. Ajitanand, et al., (2013), [arXiv:1301.0165 \[nucl-ex\]](#).
- [43] R. A. Lacey, D. Reynolds, A. Taranenko, N. N. Ajitanand, J. M. Alexander, F.-H. Liu, Y. Gu, and A. Mwai, *J. Phys.* **G43**, 10LT01 (2016), [arXiv:1311.1728 \[nucl-ex\]](#).

- [44] P. Liu and R. A. Lacey, (2018), [arXiv:1802.06595 \[nucl-ex\]](#).
- [45] R. A. Lacey, P. Liu, N. Magdy, M. Csanád, B. Schweid, N. N. Ajitanand, J. Alexander, and R. Pak, (2016), [arXiv:1601.06001 \[nucl-ex\]](#).
- [46] S. Chatrchyan et al. (CMS Collaboration), [Phys.Rev. \*\*C87\*\*, 014902 \(2013\)](#), [arXiv:1204.1409 \[nucl-ex\]](#).
- [47] S. Chatrchyan et al. (CMS), [Phys. Rev. \*\*C89\*\*, 044906 \(2014\)](#), [arXiv:1310.8651 \[nucl-ex\]](#).
- [48] S. Chatrchyan et al. (CMS), [JHEP \*\*08\*\*, 141 \(2011\)](#), [arXiv:1107.4800 \[nucl-ex\]](#).
- [49] Pifeng Liu and Roy A. Lacey, to be published.
- [50] M. L. Miller, K. Reygers, S. J. Sanders, and P. Steinberg, [Ann. Rev. Nucl. Part. Sci. \*\*57\*\*, 205 \(2007\)](#); B. Alver et al., [Phys. Rev. Lett. \*\*98\*\*, 242302 \(2007\)](#).